Table 1: Gaussian quadrature locations.

| FE order	Points on $[-1, 1]$	Points on $[0, 1]$
1	$\pm\dfrac{1}{\sqrt{3}}$	$\dfrac{1}{3+\sqrt{3}}$ $1-\dfrac{1}{3+\sqrt{3}}$
2	0 $\pm\sqrt{\dfrac{3}{5}}$	$\dfrac{1}{5+\sqrt{15}}$ 0.5 $1-\dfrac{1}{5+\sqrt{15}}$
3	$\pm\sqrt{\dfrac{3}{7}-\dfrac{2}{7}\sqrt{\dfrac{6}{5}}}$ $\pm\sqrt{\dfrac{3}{7}+\dfrac{2}{7}\sqrt{\dfrac{6}{5}}}$	$\dfrac{10+\sqrt{30}}{35+\sqrt{35(15-2\sqrt{30})}}$ $\dfrac{10-\sqrt{30}}{35+\sqrt{35(15-2\sqrt{30})}}$ $1-\dfrac{10+\sqrt{30}}{35+\sqrt{35(15-2\sqrt{30})}}$ $1-\dfrac{10-\sqrt{30}}{35+\sqrt{35(15-2\sqrt{30})}}$
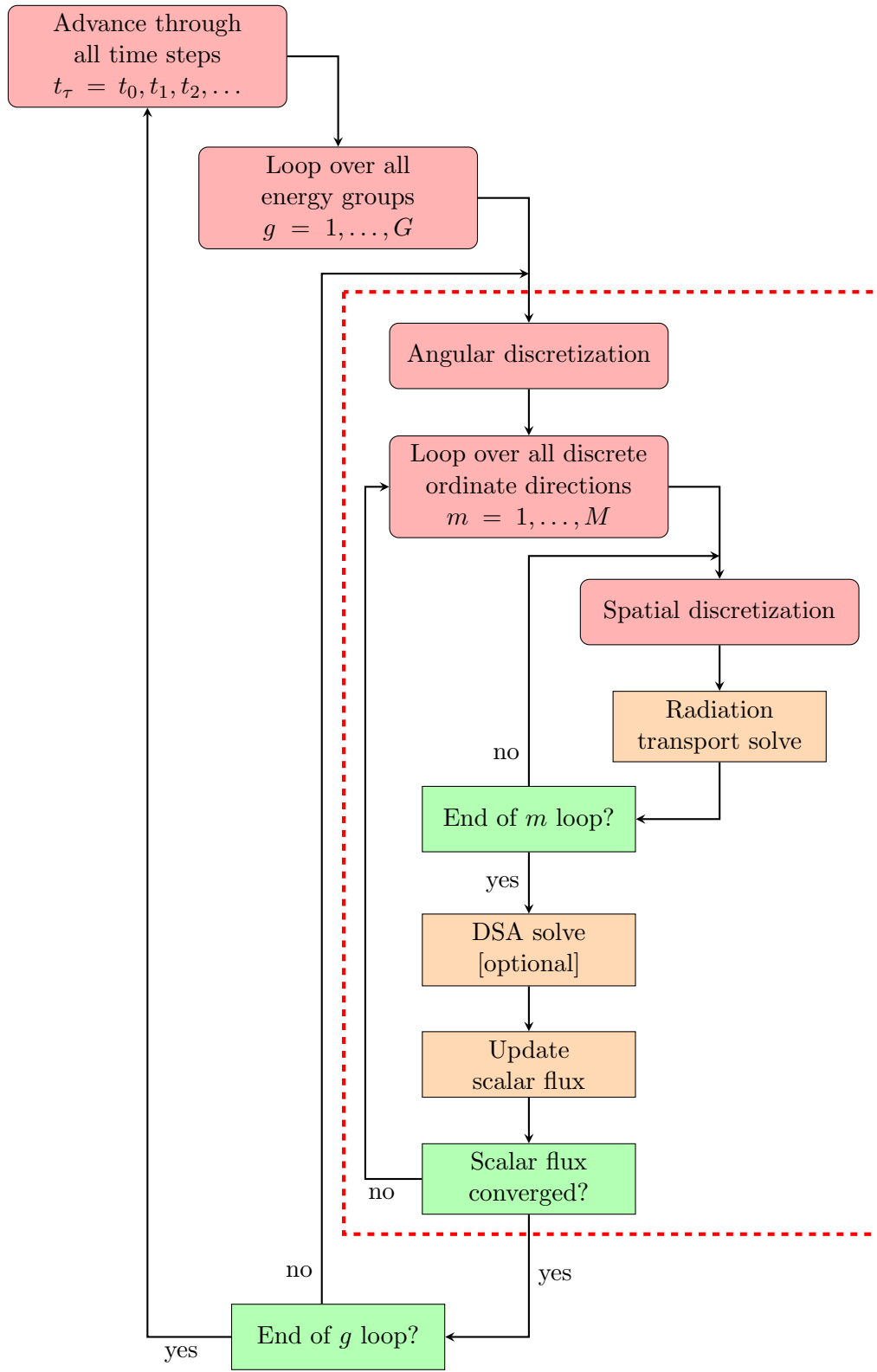
Figure 1: Flow diagram for solution process. This research is focused on the processes boxed by the dashed line.
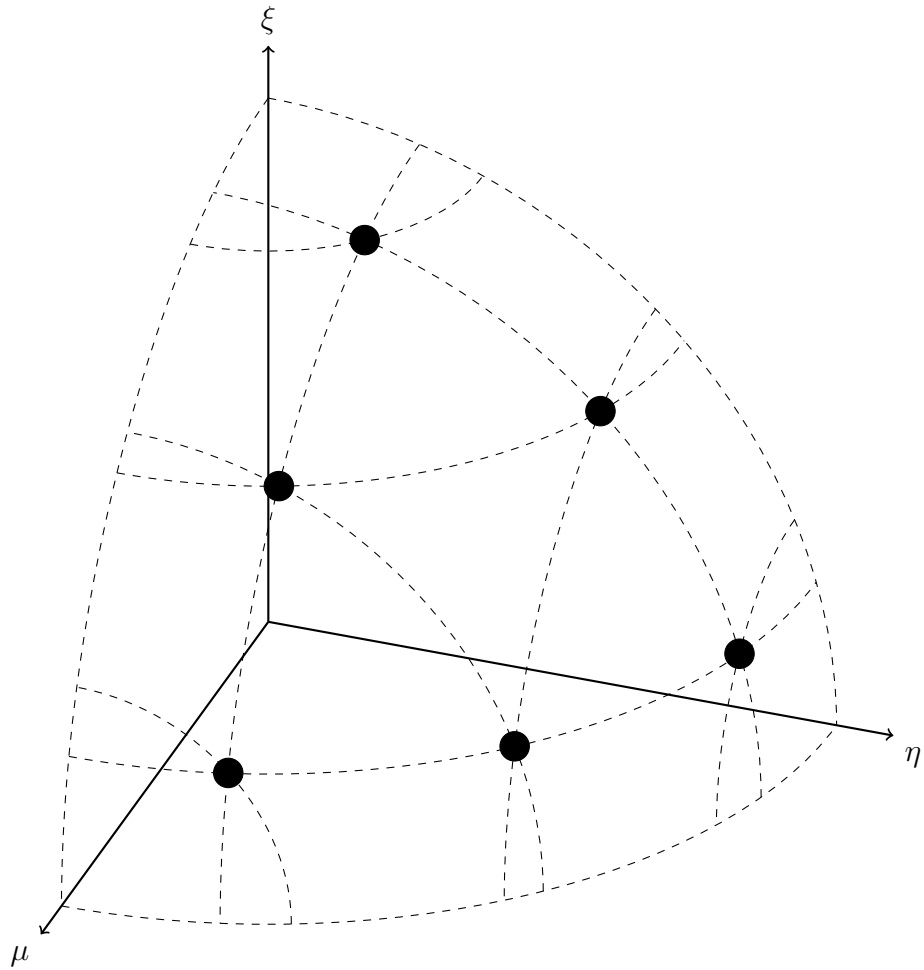
Figure 2: The positive octant for S_6 level-symmetric angular quadrature.
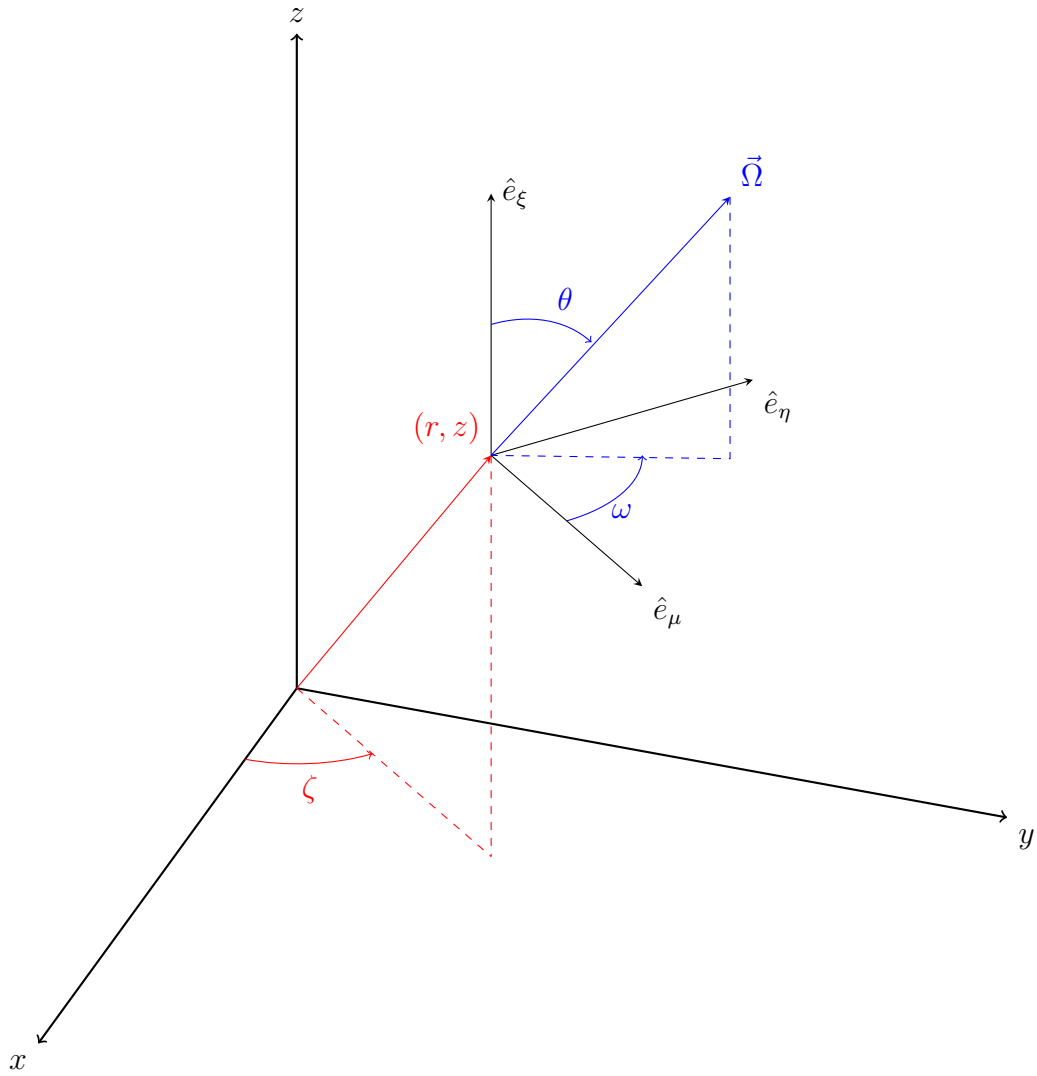
Figure 3: Cylindrical space-angle coordinate system showing the position (r, z) and direction of travel $\mathbf{\Omega}$.
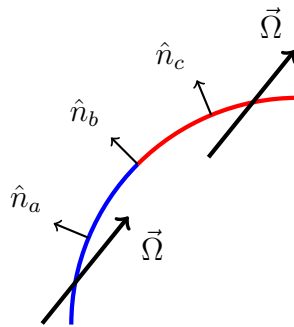


Figure 4: Example of an incident and outgoing surface.
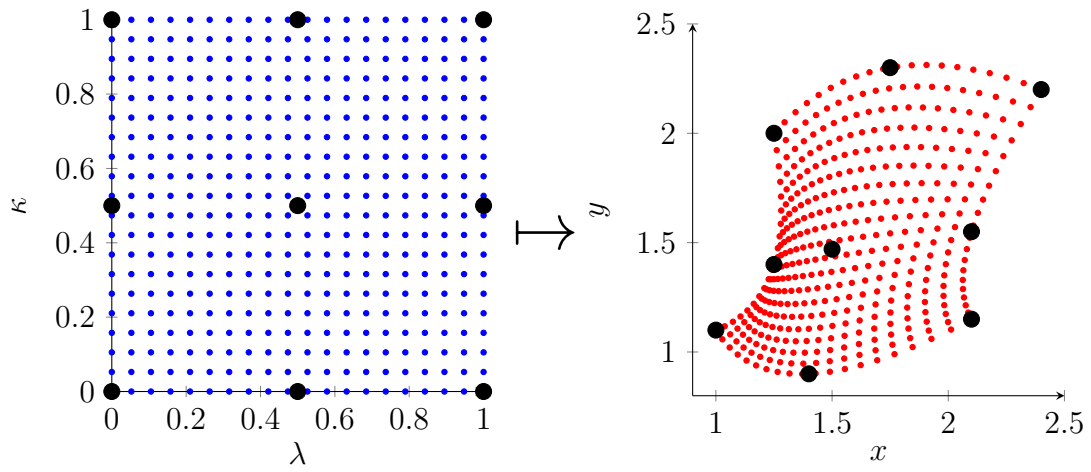
Figure 5: Example of mapping the reference element to a physical element.
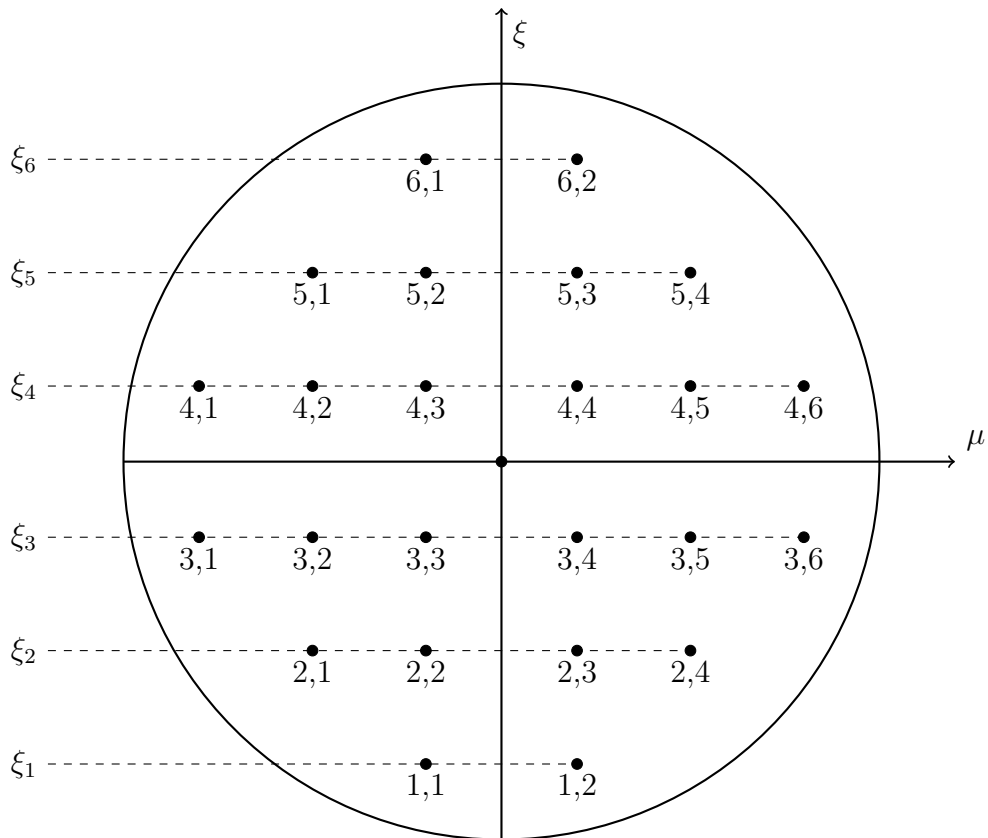
Figure 6: Angular discretization showing (ξ, μ) pairs; adapted from [**?**]

5
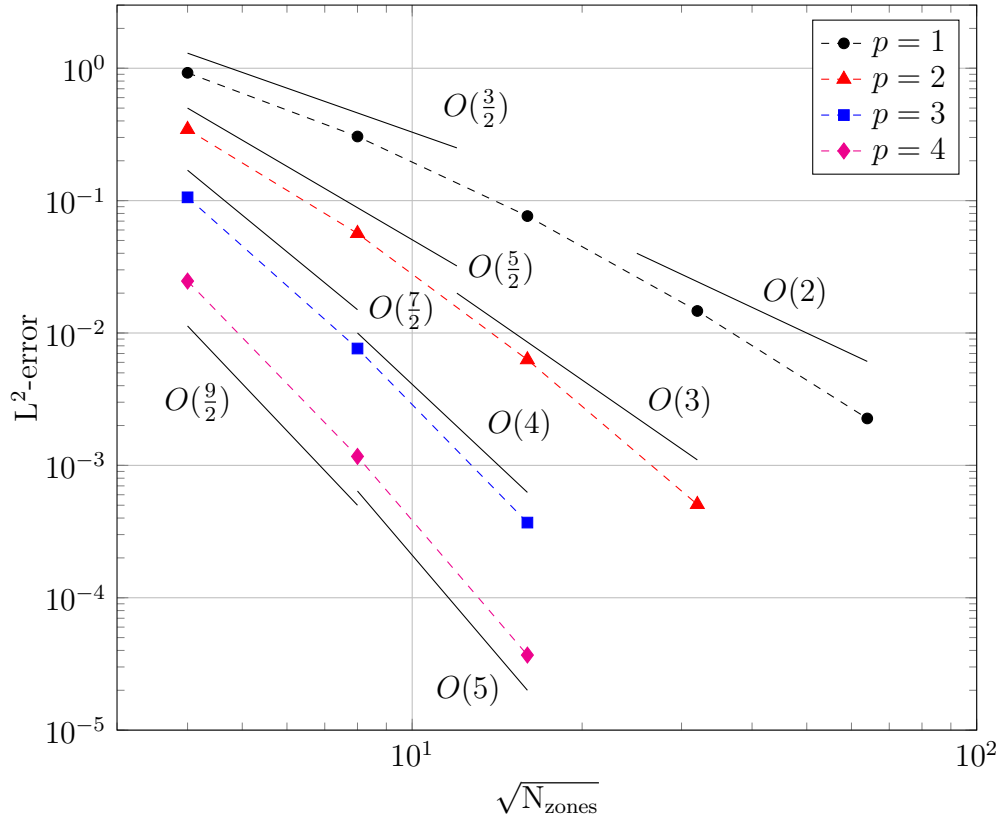
Figure 7: Errors between the manufactured and DFEM solutions. Reference lines depict order of spatial convergence $O(n) \equiv O\left((N_{\text{zones}})^{n/2}\right)$.
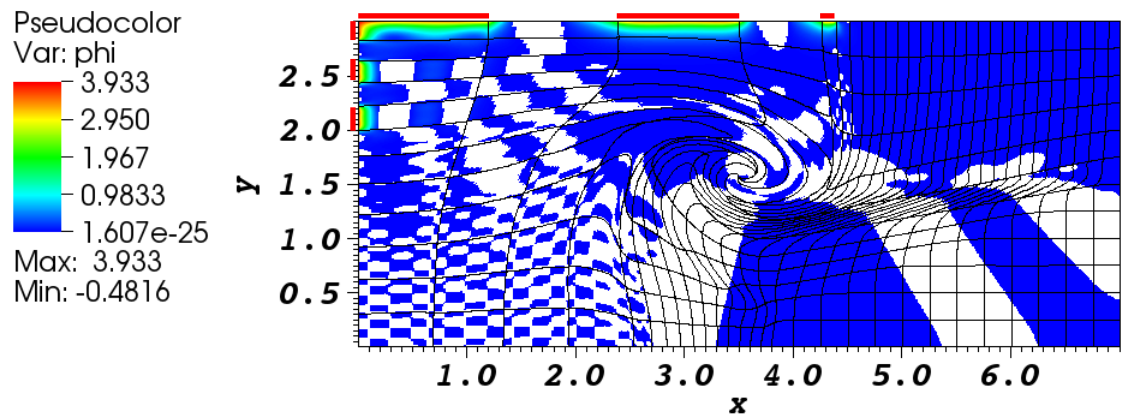
(a) Scalar flux; red bars denote incident boundary locations.
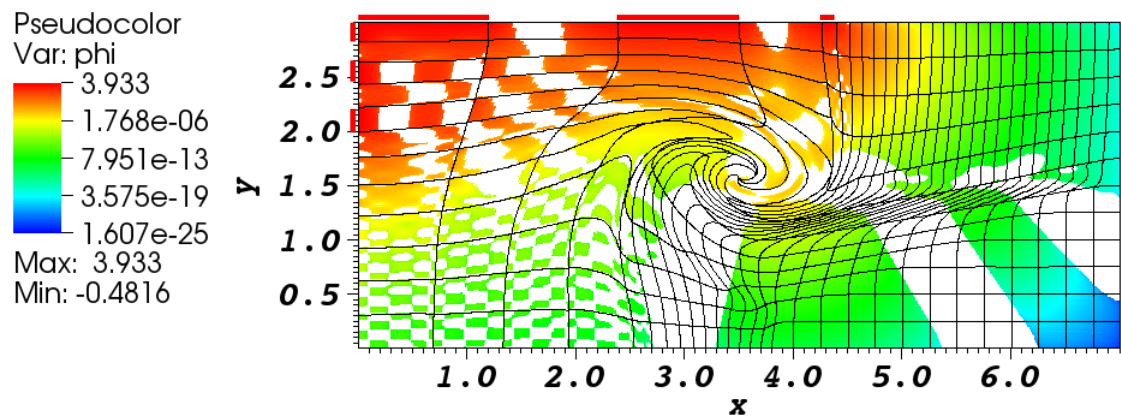
(b) Log of the scalar flux; red bars denote incident boundary locations.

Figure 8: Scalar flux solution for Test Problem 3.
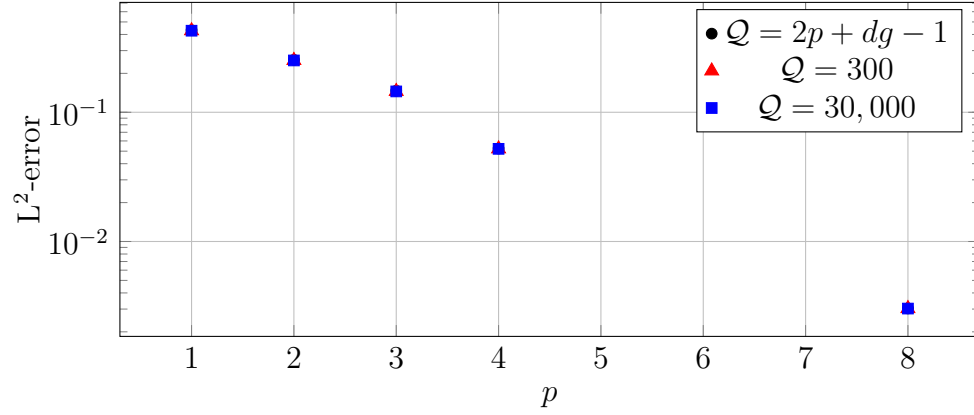
Figure 9: Error for various surface numerical integration order schemes, where p is the finite element order, g is the mesh order, and $d = 2$ is the spatial dimension of the problem.
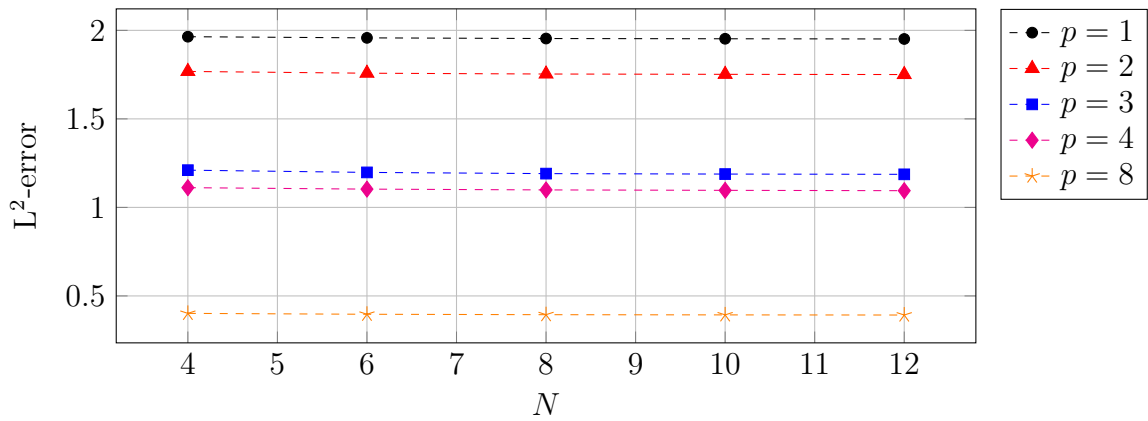
Figure 10: Error for various S_N orders.
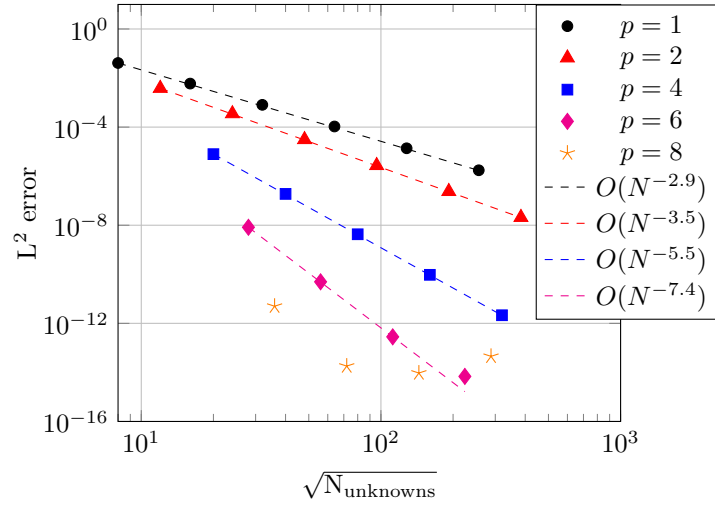
(a) Orthogonal quadrilateral mesh.
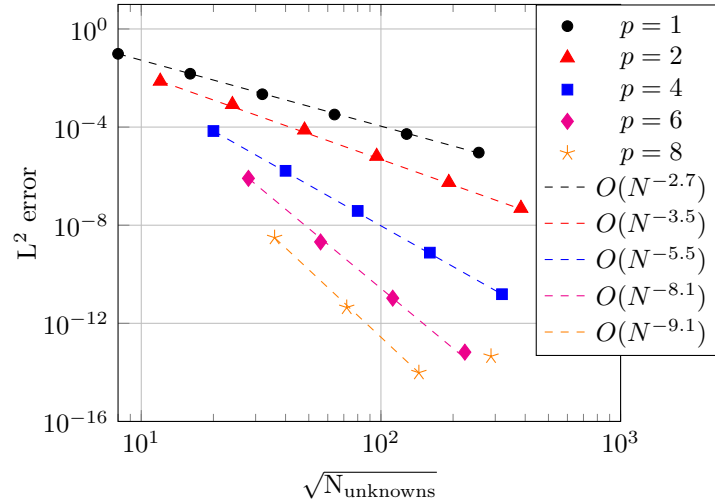
(b) 2nd-order curved mesh.

Figure 11: L^2-norm of the errors from the manufactured solution and reference lines computed from a least squares fit, where $N_{\text{unknowns}} = N_{\text{cells}}(p + 1)^2$.

9
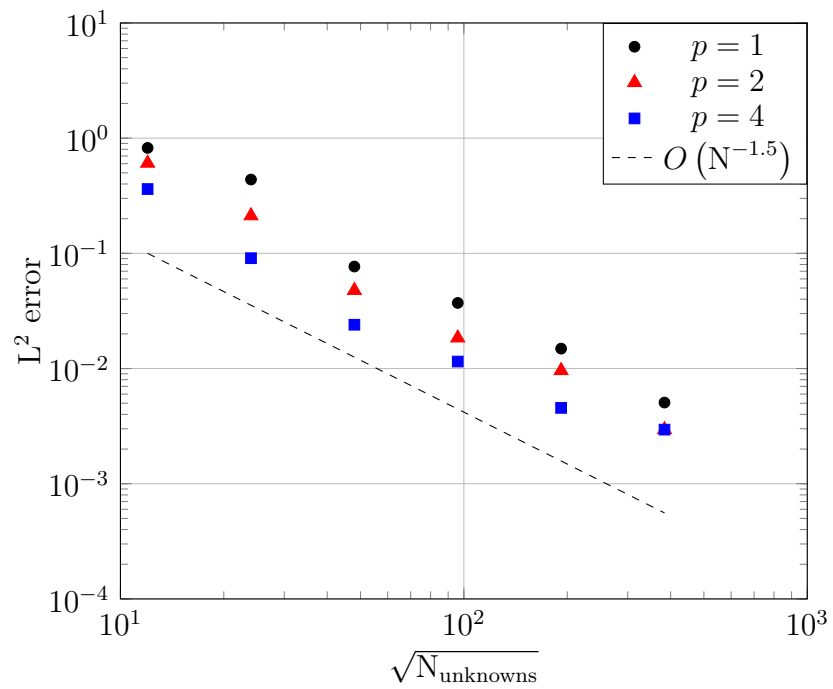
Figure 12: L^2-norm of the errors from the manufactured solution and reference line, where $N_{\text{unknowns}} = N_{\text{cells}}(p + 1)^2$.
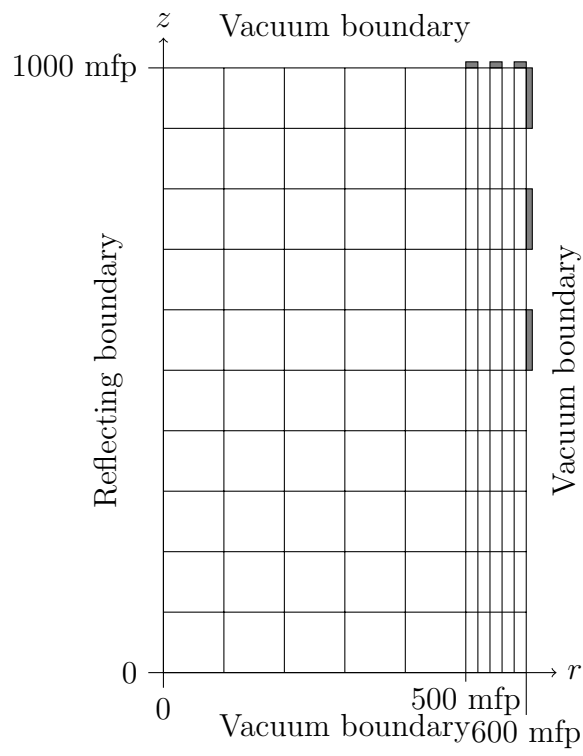
Figure 13: Strong scatter with discontinuous BCs with MIP DSA problem geometry; gray boundaries indicate incident boundary locations.
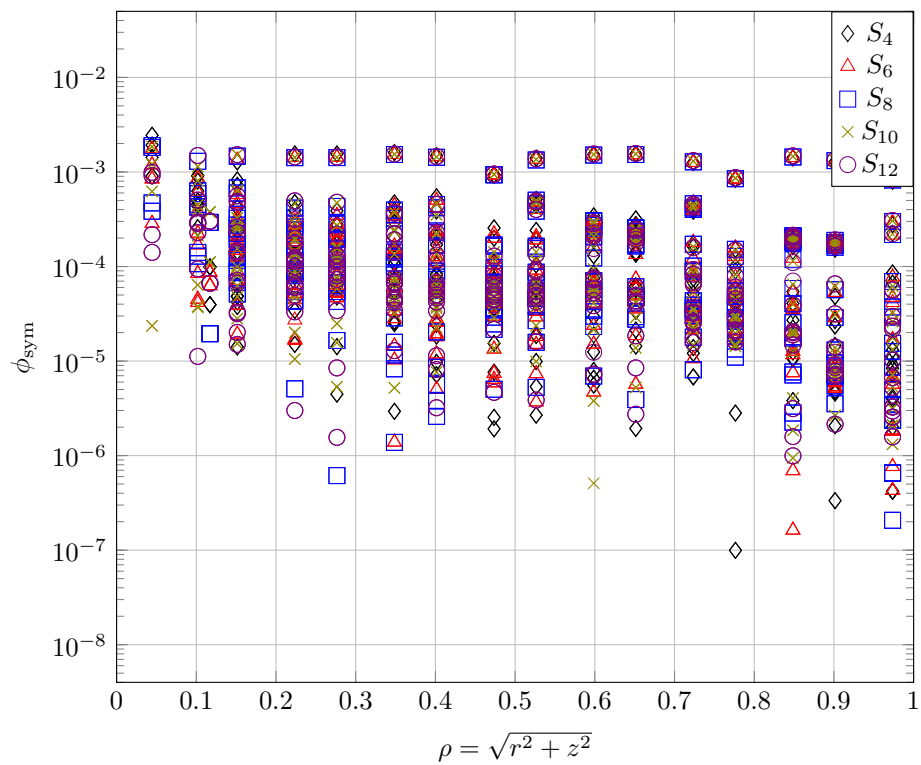
Figure 14: Measure of the asymmetry for each finite element node for the given level-symmetric angular quadrature order for 1$^{\text{st}}$-order DFEM and 1$^{\text{st}}$-order mesh with 120 zones (see Figure **??**).
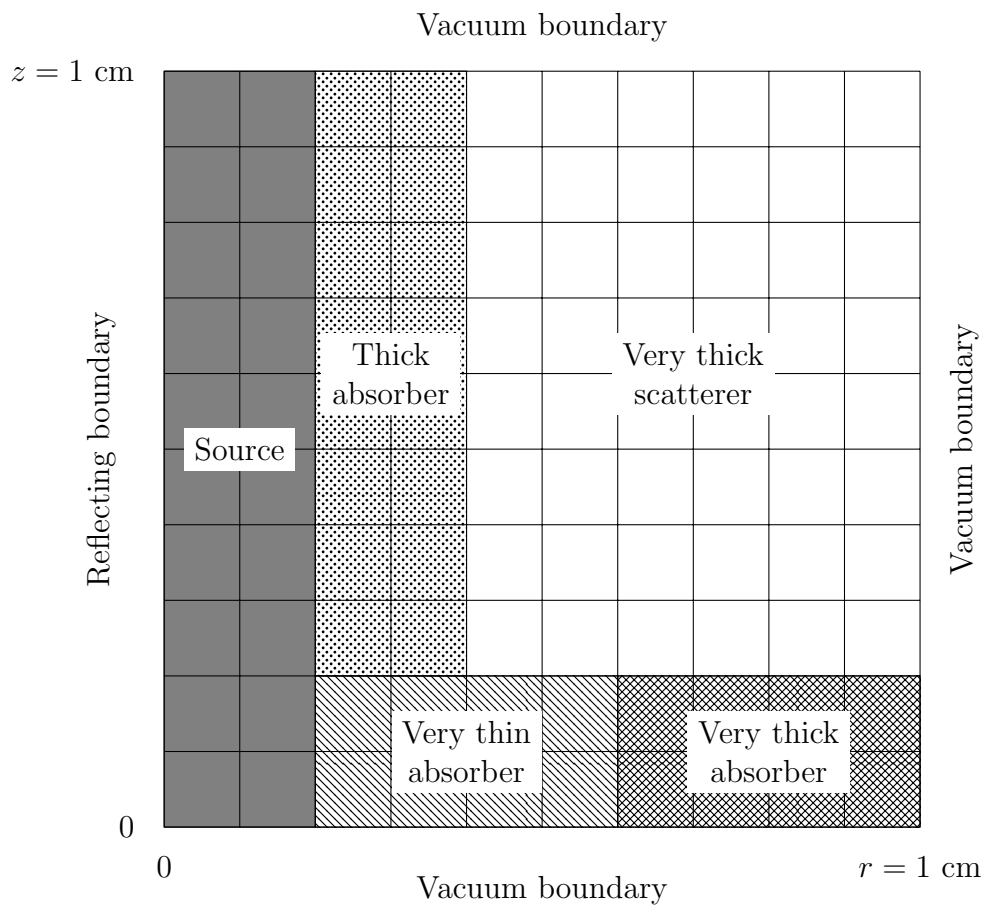
Figure 15: Material discontinuity stress test with MIP DSA problem geometry; materials defined in Table **??**.
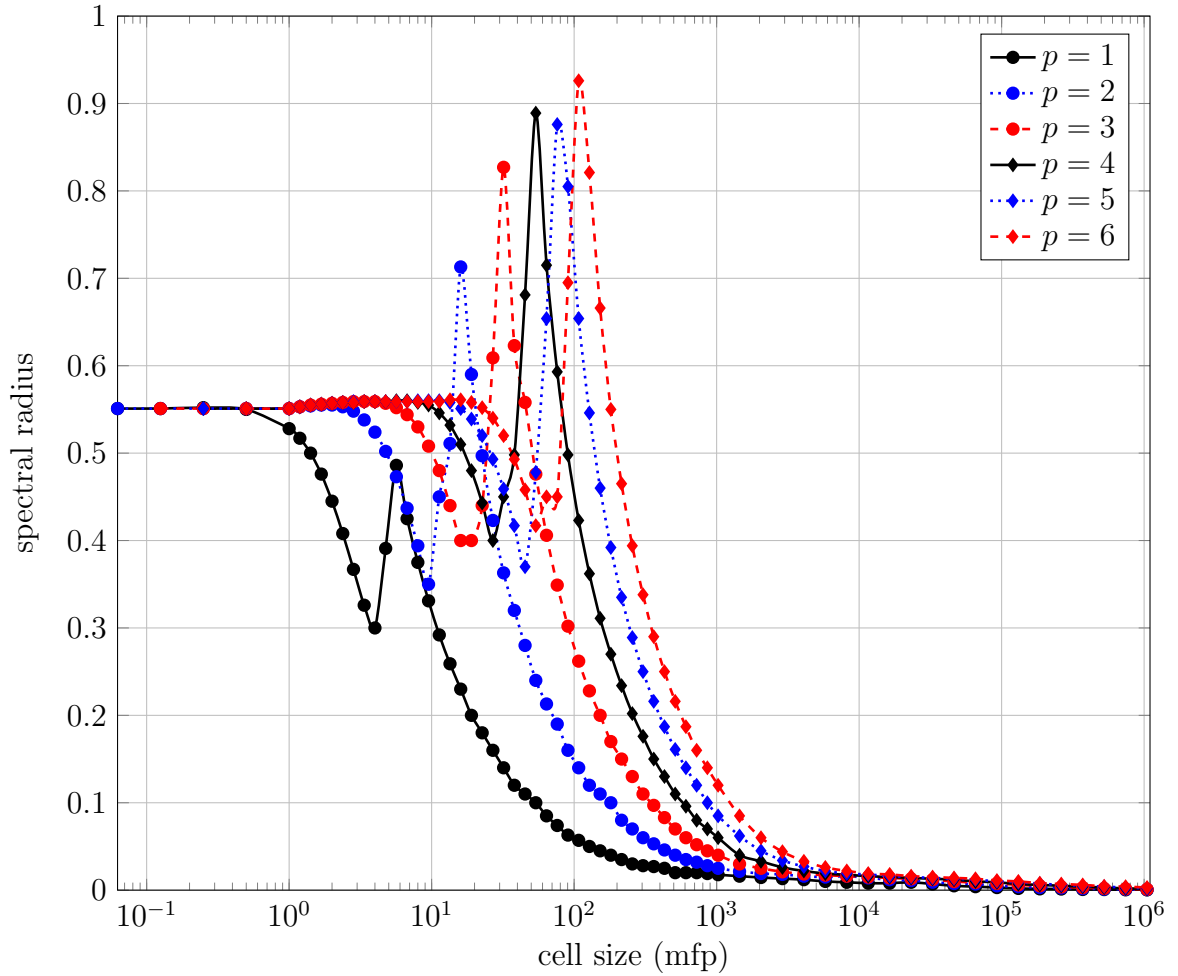
Figure 16: Spectral radius data for varying p with $C = 2$ on an orthogonal mesh with homogeneous Dirichlet boundary conditions in the DSA solve; plot reproduced from Woods et al. [?].

| no.	Discretized Equation	MFEM Equation	MFEM Integrator Function
1	$(r\,\mu_{n,m}\cdot\partial_r\,\psi_{n,m,j},\,v_i)_{\mathcal{D}_k}$ $(r\,\xi_m\cdot\partial_z\psi_{n,m,j},\,v_i)_{\mathcal{D}_k}$	$(r\,\alpha\,\boldsymbol{\Omega}\cdot\boldsymbol{\nabla}\,\psi,\,v)_{\mathcal{D}_k}$	RZConvectionIntegrator($\boldsymbol{\Omega},\alpha$)
2	$(r\,\mu_{n,m}\cdot\hat{n}\,\psi_{n,m,j},\,v_i)_{\partial\mathcal{D}_k^e}$ $(r\,\xi_m\cdot\hat{n}\,\psi_{n,m,j},\,v_i)_{\partial\mathcal{D}_k^e}$	$\alpha\,(r\,\boldsymbol{\Omega}\cdot\hat{n}\,\psi,\,v)_{\partial\mathcal{D}_k^e}$ $+\beta\,(r\,|\boldsymbol{\Omega}\cdot\hat{n}|\,\psi,\,v)_{\partial\mathcal{D}_k^e}$	RZDGTraceIntegrator($\boldsymbol{\Omega},\alpha,\beta$)
3	$(r\,\mu_{n,m}\cdot\hat{n}\,\psi_{n,m,j},\,v_i)_{\partial\mathcal{D}_k^b}$ $(r\,\xi_m\cdot\hat{n}\,\psi_{n,m,j},\,v_i)_{\partial\mathcal{D}_k^b}$	$\alpha\,(r\,\boldsymbol{\Omega}\cdot\hat{n}\,\psi,\,v)_{\partial\mathcal{D}_k^b}$ $+\beta\,(r\,|\boldsymbol{\Omega}\cdot\hat{n}|\,\psi,\,v)_{\partial\mathcal{D}_k^b}$	RZDGTraceIntegrator($\boldsymbol{\Omega},\alpha,\beta$)
4	$(\mu_{n,m}\,\psi_j,\,v_i)_{\mathcal{D}_k}$	$(\mu_{n,m}\psi,\,v)_{\mathcal{D}_k}$	MassIntegrator($\mu_{n,m}$)
5	$\left(\dfrac{\alpha_{m+1/2}^n}{\tau_{n,m}w_{n,m}}\,\psi_j,\,v_i\right)_{\mathcal{D}_k}$	$\left(\dfrac{\alpha_{m+1/2}^n}{\tau_{n,m}w_{n,m}}\psi,\,v\right)_{\mathcal{D}_k}$	MassIntegrator($\dfrac{\alpha_{m+1/2}^n}{\tau_{n,m}w_{n,m}}$)
6	$(r\,\sigma_t\,\psi_j,\,v_i)_{\mathcal{D}_k}$	$(r\,\sigma_t\,\psi,\,v)_{\mathcal{D}_k}$	RZMassIntegrator(σ_t)
7	$\dfrac{1}{4\pi}\,(r\,\sigma_s\,\phi,\,v_i)_{\mathcal{D}_k}$	$(r\,\varphi,\,v)_{\mathcal{D}_k}$	RZDomainLFIntegrator($\dfrac{1}{4\pi}\sigma_s\,\phi$)
8	$\dfrac{1}{4\pi}\,(r\,S_0,\,v_i)_{\mathcal{D}_k}$	$(r\,S_0,\,v)_{\mathcal{D}_k}$	RZDomainLFIntegrator($\dfrac{S_0}{4\pi}$)
9	$(r\,\boldsymbol{\Omega}\cdot\hat{n}\,\psi_{\text{inc}},\,v_i)_{\partial\mathcal{D}_k}$	$\dfrac{\alpha}{2}\,(r\,\psi_{inc}\,\boldsymbol{\Omega}\cdot\hat{n},\,v)_{\partial\mathcal{D}_k}$ $-\beta\,(r\,\psi_{inc}\,|\boldsymbol{\Omega}\cdot\hat{n}|,\,v)_{\partial\mathcal{D}_k}$	RZBoundaryFlowIntegrator($\psi_{inc},\boldsymbol{\Omega},\alpha,\beta$)

Table 2: MFEM *R-Z* transport operator function calls where the arguments have been dropped.